Making droplets glow in turbulence

Bocanegra Evans, Humberto; Dam, Nico; Bertens, Guus; Van De Water, Willem

DOI
10.1103/PhysRevFluids.5.044303

Publication date
2020

Document Version
Final published version

Published in
Physical Review Fluids

Making droplets glow in turbulence

Humberto Bocanegra Evans [1,2], Nico Dam [3], Guus Bertens [1,4] and Willem van de Water [1,5,*]

[1]*Physics Department, Eindhoven University of Technology, P.O. Box 513, 5600 MB Eindhoven, The Netherlands*

[2]*School of Mechanical Engineering, Purdue University, West Lafayette, Indiana 47907, USA*

[3]*Mechanical Engineering Department, Eindhoven University of Technology, P.O. Box 513, 5600 MB Eindhoven, The Netherlands*

[4]*Max Planck Institute for Dynamics and Self-Organization, Göttingen, Germany*

[5]*Laboratory for Aero and Hydrodynamics, Delft University of Technology and J.M. Burgers Centre for Fluid Dynamics, 2628 CD Delft, The Netherlands*

(Received 2 June 2017; accepted 3 March 2020; published 7 April 2020)

We present a new technique to study preferential concentration of droplets in a turbulent air flow. Preferential concentration is the tendency of droplets to cluster in regions of strain, while avoiding regions of rotation. We study the properties of the droplet concentration field in zero mean flow turbulence that was created using an array of synthetic jets. The droplets are made of a phosphorescent solution of Europium chelate. They are excited by a laser sheet from a pulsed UV laser, after which the glowing droplets are followed using a high-speed intensified camera. We quantify preferential concentration through measurement of moments of the coarse-grained local droplet density. At the Stokes numbers studied ($\mathrm{St} \approx 2$) the fractal dimension, a scaling property of this coarse-grained density field, points to clustering. Clustering is a consequence of the compressibility of the droplet velocity field. We also quantify the dynamical behavior of clustering by moving with this velocity field. We find a preference for clustering in the Lagrangian frame during the time interval set by the decay of the phosphorescence.

DOI: 10.1103/PhysRevFluids.5.044303

I. INTRODUCTION

Transport of small particles in turbulent flow is a ubiquitous phenomenon encountered in both natural and industrial processes, yet the physics governing these situations remains unclear. Many questions regarding the effects of turbulence on suspended particles have been addressed in the past few years with the help of numerical simulations and advanced experimental techniques (see Refs. [1–3] and references therein); however, many remained unanswered.

In this paper we describe a new method to study the evolution of the concentration field of droplets suspended in a turbulent flow. At initial time, a sheetlike volume of droplets is tagged by briefly (5 ns) illuminating them with a laser pulse from a UV laser. The droplets contain a phosphorescent solution of a Eu-based lanthanide chelate and glow long enough to follow them during a few Kolmogorov times. The Kolmogorov timescale τ_η is the turnover time of the smallest eddies in turbulence, which in this experiment is approximately half a millisecond. The droplets are followed during a few milliseconds using a fast intensified camera. This is repeated many times, so that adequate statistics of the evolving concentration field is gathered.

*Corresponding author: w.vandewater@tudelft.nl; present address: Laboratory for Aero and Hydrodynamics, Delft University of Technology and J.M. Burgers Centre for Fluid Dynamics, 2628 CD Delft, The Netherlands.

Glowing droplets can be used in a number of different ways, for example to estimate the concentration of particles by tracking the signal intensity as will be done in this paper, or by measuring the size evolution of small tagged volumes for a study of the dispersion of droplets, as was done by Ref. [4]. Additionally, this technique may be integrated into particle tracking methods, to follow only a specific set of particles in dense clouds.

Preferential concentration is a phenomenon observed in particle- and bubble-laden flows due to inertial effects of the dispersed phase [5,6]. For heavy particles, inertia prevents them from faithfully following the flow, filtering out the strongest fluctuations in the acceleration [7] and creating singularities (caustics) in their distribution [8–10]. These inertial effects create concentration inhomogeneities with particles being expelled from vorticity-dominated regions and agglomerating in strain-dominated ones (the sling effect). Inertia is quantified by the Stokes number $\mathrm{St} = \tau_p/\tau_\eta$, where τ_p is the particle relaxation time. The particle relaxation time τ_p is determined by Stokes friction, and defined as $\tau_p = \rho_p d_p^2/18\mu$, where d_p is the droplet diameter, ρ_p the liquid mass density, and μ the dynamic viscosity of air. The smallest time and length scales of the flow are defined using the energy dissipation rate ε and the kinematic viscosity ν of air $\tau_\eta = (\nu/\epsilon)^{1/2}$ and $\eta = (\nu^3/\epsilon)^{1/4}$.

Preferential concentration is most outspoken for Stokes numbers close to one, where the particle relaxation time is comparable to the Kolmogorov time. It is our aim to design an experimental diagnostic that allows us to observe the dynamics of preferential concentration on the smallest relevant length and timescales of the flow. At the turbulence conditions realized in this experiment, $\tau_\eta \approx 0.5$ ms, which calls for small droplets, $d_p \approx 13$ μm, to make $\mathrm{St} = 1$ in air.

A key question in cloud physics is how the droplet size distribution evolves under the influence of collisions. In a kinetic equation, collisions are quantified by the collision kernel, which is determined by the probability to find two droplets at a distance where they touch, and by their relative velocities. The chance to find two droplets at a distance r is quantified by the radial distribution function $g(r)$. The one-dimensional version of the radial distribution function $g_{1\mathrm{D}}(r)$ was measured by Saw *et al.* [11] in strong ($\mathrm{Re}_\lambda = 440$–$800$) homogeneous, isotropic wind-tunnel turbulence. The Stokes numbers were small ($\mathrm{St} = 0.01 \ldots 1$) and the experimental correlation functions were obtained using Taylor's frozen turbulence hypothesis. At large r insufficient mixing time of the injected droplets prevented the correlation functions to reach the asymptote $g_{1\mathrm{D}}(r \to \infty) = 1$. Clustering was most evident at scales $\lesssim 10\eta$, and a strong dependence of $g_{1\mathrm{D}}(r)$ on the Stokes number was found. Good agreement was found with numerical simulations at $\mathrm{Re}_\lambda = 143$ [12]. At small separations, a power law $g_{3D}(r) = c_0(\eta/r)^{c_1}$ was observed with the clustering exponent c_1 asymptotically reaching a value $c_1 \approx 0.7$ at $\mathrm{St} \approx 1$. [13] measured radial distribution functions $g_{3D}(r)$ from droplet coordinates obtained holographically in a turbulent flow at $\mathrm{Re}_\lambda = 108 \ldots 147$ stirred by 8 fans in the corners of a box with linear dimension 0.38 m; a device similar to ours. Also in this experiment the Stokes numbers were small, $\mathrm{St} = 0.21 \ldots 0.60$, with the corresponding clustering exponents $c_1 = 0.25 \ldots 0.40$.

Preferential concentration leads to a droplet distribution with voids and clusters. Such a distribution resembles a fractal, which is characterized by structure at all scales. It can be quantified by counting the number of droplets $N(\delta)$ in boxes with increasing linear size δ. In case of a homogeneous distribution in three dimensions, $N(\delta) \propto \delta^D$, with dimension $D = 3$. However, if the particles agglomerate, then the dimensionality of the droplet distribution is reduced; Calzavarini *et al.* [14] found a fractal dimension of $D \approx 2.4$. This number was reached in two different ways: by viewing the motion of a single droplet as a six-dimensional dynamical system, a fractal dimension can be computed from the associated Lyapunov exponents using the conjecture of Kaplan and Yorke [15]. Alternatively, the correlation fractal dimension was also computed from the spatial droplet distribution.

Other box-counting measurements have been performed by Bec *et al.* [16], where the probability density function of the number of particles per box showed longer tails compared to that of a random distribution as a result of voids and clusters. The deviation from randomness, characteristic of clustered particle suspensions, was also found by Monchaux *et al.* [17], who analyzed the particle

distribution using Voronoi tesselation and compared the inertial particle distribution to that expected of tracers, finding a large amount of clusters and voids.

While the radial distribution function and the fractal dimension quantify the distribution of droplets in snapshots, very few experimental studies exist that quantify the dynamics of clustering. An exception is the work by Bewley *et al.* [10] who, in pursuit of the sling effect, analyzed gradient dynamics of the droplet velocity field $\boldsymbol{v}(\boldsymbol{x}, t)$ in volumes that were only a few Kolmogorov lengths large.

As is well known, the velocity field $\boldsymbol{v}(\boldsymbol{x}, t)$ of inertial particles is compressible,

$$\boldsymbol{\nabla} \cdot \boldsymbol{v} = -\tau_p \boldsymbol{\nabla} \cdot (\boldsymbol{u} \cdot \boldsymbol{\nabla} \boldsymbol{u}), \tag{1}$$

where $\boldsymbol{u}$ is the turbulent velocity, and τ_p is the Stokes time. By separating the field $\boldsymbol{\nabla u}$ in Eq. (1) into strain and rotation components, it readily follows that the particle velocity field $\boldsymbol{v}$ is compressible in regions of strain. The particle density field $n(\boldsymbol{x}, t)$ satisfies the continuity equation,

$$\frac{\partial n}{\partial t} + \boldsymbol{\nabla} \cdot (\boldsymbol{v}\, n) = 0, \tag{2}$$

where we have ignored diffusion (Brownian motion) of the droplets. In the Lagrangian frame,

$$\frac{dn}{dt} = -n(\boldsymbol{\nabla} \cdot \boldsymbol{v}), \tag{3}$$

such that the density n grows in regions of strain. Droplet clusters are singled out by the positive moments $\langle n^\alpha(t)\rangle$ with $\alpha > 0$, of the local density field. Formally, the compressibility of the droplet velocity field can only be proven for small Stokes numbers. However, the result is consistent with the sling effect and emphasizes the Lagrangian frame for understanding droplet clustering.

The quantity $-\boldsymbol{\nabla} \cdot \boldsymbol{v}$ plays the role of a fluctuating finite-time Lyapunov exponent in the theory of dynamical systems. Balkovsky *et al.* [18] argue that over time intervals much longer than the correlation time of the turbulent velocity field, $\langle n^\alpha(t)\rangle$ increases exponentially. These times are out of reach in our experiments where the phosphorescence only lives a few Kolmogorov times, but we are still able to distinguish the dynamical behavior of density moments in the Eulerian and Lagrangian frame.

Our experimental method allows measurement of $\langle n^\alpha(t)\rangle$ both in the Eulerian, $\langle n^\alpha(t)\rangle_E$ and in the Lagrangian $\langle n^\alpha(t)\rangle_L$ frame, and we will show the ratio $\langle n^\alpha(t)\rangle_L / \langle n^\alpha(t)\rangle_L$. In the Eulerian case, averages $\langle \ldots \rangle$ are just done over squares that fill the tagged sheet. These squares remain stationary as time progresses. In the Lagrangian case these squares, also filling the sheet at the instant of tagging $t = 0$, go with the flow at later times $t > 0$.

Both quantities, the fractal dimension and the evolution of clusters, are a property of the concentration field of the droplets. We do not resolve individual droplets, but because our droplets are close to monodisperse, the measured phosphorescent light intensity is proportional to the droplet concentration. Therefore, our experimental method is suited well for the measurement of these quantities.

Our experiment is in the realm of molecular tagging velocimetry, a full description of which is given in Sec. II. The turbulence chamber and the characteristics of the generated turbulence are discussed in Sec. III. Our results in Sec. IV are for the fractal dimensions and the temporal evolution of the density moments.

II. PHOSPHORESCENCE TAGGING

Using glowing droplets to probe preferential concentration in turbulence is related to the well-known technique of molecular tagging velocimetry (MTV), in which marked molecules are used to trace the flow that carries them. This marking differentiates them from other molecules, including those that make up the fluid or the gas. Examples are the photoactivation of caged fluorescent molecules in a liquid, first proposed by Lempert *et al.* [19]. In flows of gases, several techniques have been described to either excite molecules to a metastable state [20,21] or to create tracer molecules

by photoactivated chemistry [22,23]. An extensive review on MTV is given by Koochesfahani and Nocera [24].

MTV is based on the *generation* of tracers within the fluid. That is, the fluid itself is locally transformed, photophysically or otherwise, into a tracer which is made from the same composition as the fluid. Many variations of MTV exist, with the first option being the choice between fluorescence and phosphorescence. Depending on the timescales of the particular experiment at hand, one must decide what type of luminescent solution to use. Both fluorescence and phosphorescence have been used previously for flow diagnostics. The former has the advantage of an immediate and relatively strong light emission. The latter prolongs the luminescence duration at the expense of its intensity. Also, gas or liquid can be used as the working fluid.

Our aim is a study of preferential concentration in turbulence, using phosphorescent droplets. This method is inspired by Krüger and Grünefeld [25] who used a similar technique, but with another molecular tracer, to measure the velocity field of dispersed droplets using a grid of laser beams. The deformation of the resulting grid of glowing molecules was measured using a correlation technique similar to the one used in particle image velocimetry.

The turbulence in our experiment is characterized by a smallest eddy turnover time $\tau_\eta = 0.5$ ms, which requires a phosphorescence life time of the tagged droplets of a few times τ_η (a few ms), to be able to follow the dynamics of preferential concentration. In addition, the small volume of the St ≈ 1 droplets necessitates maximization of the phosphorescence intensity.

In our experiment, the droplets are made from a water-based Europium solution, with the Europium ions organised in a chelate. The structure of the chelate consists of a "cage" created by one or more ligand molecules which contains the Europium ion (Eu^{+3}). This cage, however, does not impede the phosphorescence of the lanthanide. On the contrary, the ligands act as antennae that absorb laser light and transfer the excitation to the Eu-ion, which in turn emits photons of a specific wavelength, 614 nm in the present case [26]. The ratio of concentrations of ligands and lanthanide has an impact on the phosphorescence intensity [27].

The ligands used in this solution were thenoyltrifluoroacetone (TTA), which has a broad absorption peak around 365 nm, and trioctylphosphine oxide (TOPO). Although the stoichiometric composition of the solution was found to be $Eu(TTA)_3(TOPO)_2$ by Arnaud and Georges [27], they also concluded that phosphorescence reached a maximum when the concentration of TTA was at least ten times that of Europium. Since a stronger phosphorescent signal allows for a longer tracking of the droplets, the solution used in the present study was prepared with large TTA concentration.

Stock solutions for each of the three components were mixed separately. The Europium stock solution used distilled water as a solvent and Europium(III) chloride hexahydrate, while the TTA and TOPO solutions used ethanol; all stock solutions have a concentration of 10^{-2} M. The dilute solution was then prepared by mixing distilled water with the necessary amount of each solution. The final concentration of the solution was 8.3×10^{-5}M Eu^{+3}, 8.3×10^{-4}M TTA, 8.3×10^{-4}M TOPO. Finally, to clear the solution and serve as a wetting agent, 0.1% by volume of Triton X-100 was added.

The decay time of the phosphorescent solution was measured by illuminating droplets using frequency-tripled Nd:YAG laser pulses and recording the decay of the phosphoresence intensity. It varied between 500 and 800 μs, giving us the opportunity to image the particles during approximately $4\tau_\eta$. A typical decay curve is shown in Fig. 1(a). With the aim of increasing the quality of the recorded images we inspect the dependence of the emission strength on the laser power. As shown in Fig. 1(b), the phosphorescent signal saturates as the laser power is increased. Multiple scattering may contribute to tagging, with the effect of widening of tagged volumes. Therefore, the laser power must be chosen judiciously.

III. EXPERIMENTAL SETUP AND PROCEDURE

The goal of our experiments is to measure preferential concentration of heavy particles in a turbulent flow using the new diagnostic of glowing droplets. Homogeneous, isotropic turbulence

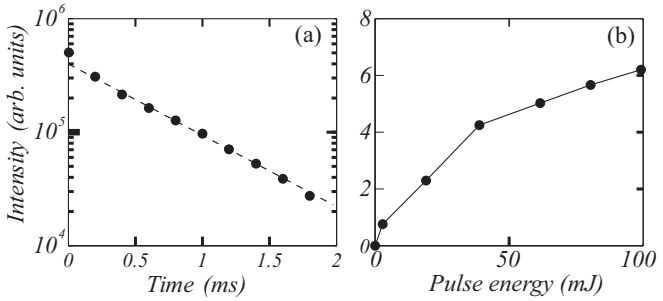

FIG. 1. (a) Exponential decay of the phosphorescent signal of a collection of droplets. It was measured by registering the intensity with a fast camera after illumination with the laser at $\tau = 0$; an average over 2400 laser pulses is shown. The decay time is $\tau_{\mathrm{ph}} = 710\ \mu$s. (b) Saturation of the phosphorescence intensity with increasing laser power (Nd:YAG laser at 355 nm).

with zero mean flow was created in a box using an array of synthetic jets, in an arrangement inspired by the work of Hwang and Eaton [28]. A spinning disk droplet generator is used to fill the box with a mist of phosphorescent droplets.

A. Turbulence chamber

The design of the turbulence chamber takes advantage of the property synthetic jets possess in which momentum transfer is possible without mass transfer occurring, in an average sense. The apparatus consists of a PVC cubic box with truncated corners, each fitted with speaker-driven synthetic jets. Hwang and Eaton [28] were able to reach $\mathrm{Re}_\lambda = 218$, in our setup we reach $\mathrm{Re}_\lambda = 563$. In this way, the inertial range is widened, and the Kolmogorov timescale τ_η is shortened, so that droplets can be tracked for a few τ_η during their phosphorescent lifetime. The box, which is shown in Fig. 2, has a side length of 400 mm and speakers of 365-mm diameter (MTX Audio sub-woofer model RT15-04, Mitek Corporation, Phoenix, AZ). Optical access was available on four of its six sides through perspex windows.

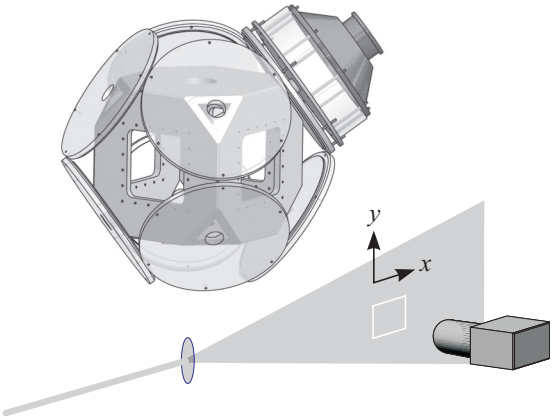

FIG. 2. Model of turbulence chamber, with arrangement of light sheet and camera. For clarity, only one speaker is shown. The inner side length of the chamber is 40 cm. The jet orifices have a diameter of 4 cm. For the measurement of the concentration field, the camera images a square with size 32×32 mm^2.

The synthetic jets point toward the center of the box, and are driven independently with random voltages generated by series of independent pseudorandom numbers. By employing a Gaussian filter, the driving voltages have a broad spectrum, $E(f) \propto \exp[-(f - f_0)^2/\sigma^2]$ with center frequency $f_0 = 40$ Hz and spectral width $\sigma = 19$ Hz. The eight instantaneous driving voltages add to 0, so that the pressure in the chamber stays approximately constant.

The driving voltages were generated using a 16-bit, eight-channel analog output card (model 16AO16, General Standards Corp., Huntsville, AL) which has sample buffers large enough to allow uninterrupted generation of the driving voltages. Those voltages were transmitted to eight amplifiers (model RN-2160, Rodek, Garden Grove, CA). Slight differences in speaker performance resulted in a mean flow. Added to this, the aerosol generator used for the production of the phosphorescent droplets also induced a mean flow. To counteract these effects, speaker-specific coefficients were implemented in the driving algorithm, allowing fine tuning of the synthetic jets.

B. Flow characterization

Particle image velocimetry was used for the turbulence characterization, allowing a 2D measurement of the velocity. The PIV setup consisted of a dual-head Nd:YAG laser (CFR400, Quantel) and a 1600×1200 pixel^2 digital camera (ES2020, RedLake). Seeding for the PIV measurements was done with a commercial smoke generator capable of producing droplets of approximately 1 μm. The region of view was approximately 60×80 mm^2 (resulting in a magnification of 20 pixel/mm), and the sampling rate was 15 Hz. The processing was done with commercial software (PIVtec, Göttingen, Germany) using a 32×32 pixel interrogation area with a 50% overlap.

A challenge of the setup is achieving homogeneous turbulent flow with zero mean velocity. This required balancing the rms amplitude of the loudspeaker signals. To this aim, a series of short PIV measurements in two perpendicular planes was performed to fine tune the speaker power. Once satisfactory flow conditions were reached, an extended measurement was performed to characterize the turbulence, for which approximately 1500 2D PIV fields were obtained.

The mean and fluctuating velocity fields are shown in Fig. 3, where we also indicate the region of interest of the droplet tagging experiments. The balancing of the synthetic jets is not perfect and inside the region of interest a mean velocity of approximately 10% of the fluctuating velocity remains. Over the entire 78×58 mm^2 field of view, the total fluctuating velocity, $(u^2 + v^2)^{1/2}$ ranges from $\approx 2.3 - 3.0$ m/s, but inside the region of interest of the tagging experiments, the homogeneity is much better.

The turbulence characteristics were inferred from the PIV measurements. As PIV involves averaging of the velocity field over the interrogation windows, a direct measurement of gradients at the smallest scales, needed for the computation of the turbulent dissipation rate ε, underestimates the magnitude of these gradients. We have used a model to correct for this intrinsic averaging [29,30]. This procedure relies on the Smagorinsky model [31] for the calculation of the subgrid stresses.

In addition, we have estimated ε from measured second- and third-order structure functions. These structure functions are shown in Fig. 4. With two components of the velocity field measured in the x y plane, the longitudinal second-order structure functions are $G^x_{xx}(r) = \langle [u(\boldsymbol{x} + r\boldsymbol{e}_x) - u(\boldsymbol{x})]^2 \rangle_{x,y}$ and $G^y_{yy}(r) = \langle [v(\boldsymbol{x} + r\boldsymbol{e}_y) - v(\boldsymbol{x})]^2 \rangle_{x,y}$, while the transverse structure functions are $G^y_{xx}(r) = \langle [u(\boldsymbol{x} + r\boldsymbol{e}_y) - u(\boldsymbol{x})]^2 \rangle_{x,y}$ and $G^x_{yy}(r) = \langle [v(\boldsymbol{x} + r\boldsymbol{e}_x) - v(\boldsymbol{x})]^2 \rangle_{x,y}$. For the third-order structure functions, the only non-zero ones are G^x_3 and G^y_3, with the velocity components and the separation vector pointing in the same direction.

Due to the inhomogeneity of the velocity field, third-order structure functions are difficult to measure. Therefore, we have removed some of the inhomogeneity by normalizing the velocity field by first subtracting the (small) mean field, and then normalize $\boldsymbol{u}(\boldsymbol{x}) \langle \langle \boldsymbol{u} \cdot \boldsymbol{u} \rangle \rangle^{1/2}_{x,y} / \langle \boldsymbol{u} \cdot \boldsymbol{u} \rangle^{1/2}$ where $\langle\rangle$ denotes a time average and $\langle\langle\rangle\rangle$ both space- and time averages.

From a direct measurement of the velocity gradients, which are measured using a least-squares differentiation formula [30], we obtain $\varepsilon = 54$ m^{2}s^{-3}, while the second-order structure functions were fitted with $G_2^{L\,x,y}(r) = C_2\, \varepsilon^{2/3} r^{2/3}$, with $\varepsilon = 64$ m^{2}s^{-3}, and the third-order structure functions

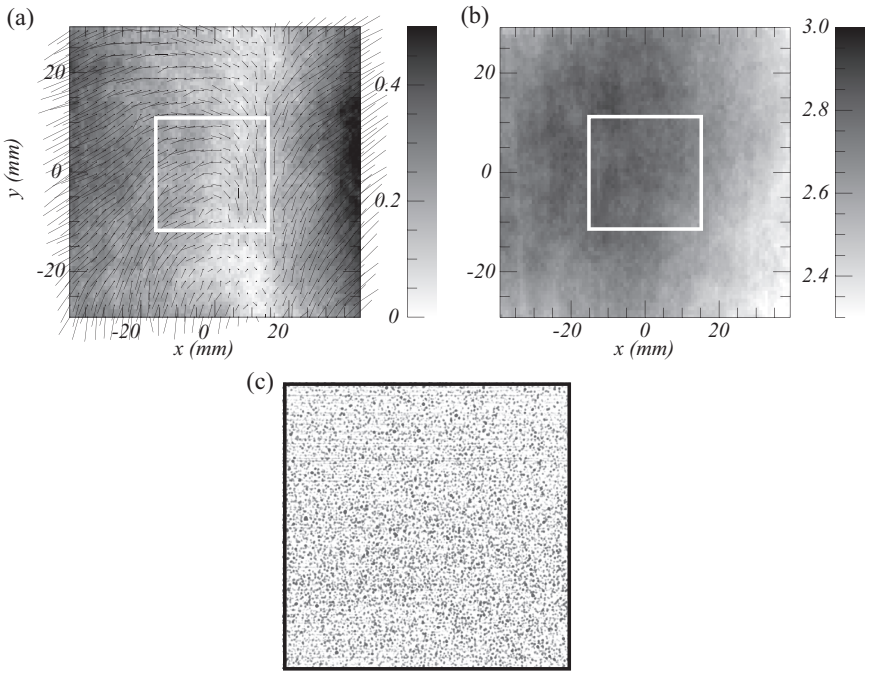

FIG. 3. (a) Mean velocity field and (b) gray-scale plot of the total fluctuating velocity $(u^2 + v^2)^{1/2}$, measured using particle image velocimetry. (c) Snapshot of the tagged sheet 3 μs after tagging. The droplet tagging experiments have a smaller field of view, indicated by the squares in (a), (b).

were fitted with $G_3^{x,y} = -(4/5)\varepsilon\, r$, with $\varepsilon = 56\ \mathrm{m^2 s^{-3}}$. The fit of the second-order structure function overestimates ε due to the averaging which is intrinsic to the PIV procedure. Therefore, we adopt the value $\varepsilon = 54\ \mathrm{m^2 s^{-3}}$. With a measured turbulent velocity $u = 1.9$ m/s, we obtain a Taylor microscale Reynolds number $\mathrm{Re}_\lambda = 490$, and Kolmogorov time- and length scales $\tau_\eta = 5.3 \times 10^{-4}$ s and $\eta = 89\ \mu$m, respectively. Together with the mean droplet diameter $d_p = 18\ \mu$m, this leads to a Stokes number $\mathrm{St} = 1.9$. Finally, the turbulent velocity field, is isotropic to within 10%, both at large and small scales [30]. The phosphorescent tagging experiments were carried out independently from the flow characterization (PIV) experiments, under the assumption that the presence of the dispersed phase has a negligible impact on the characteristics of the flow.

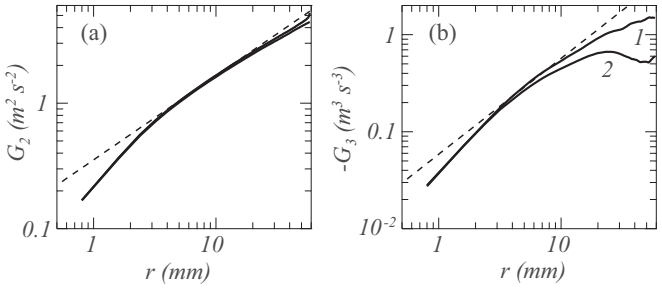

FIG. 4. (a) Full lines show the second order longitudinal structure functions $G_{xx}^x(r)$ and $G_{yy}^y(r)$. The dashed line is $G_{xx}^x(r) = G_{yy}^y(r) = C_2\, \varepsilon^{2/3} r^{2/3}$, with $\varepsilon = 64\ \mathrm{m^2 s^{-3}}$. (b) Full line 1 is $-G_3^x$; line 2 is $-G_3^y$. The dashed line is $G_3^{x,y} = -(4/5)\varepsilon\, r$, with $\varepsilon = 56\ \mathrm{m^2 s^{-3}}$.

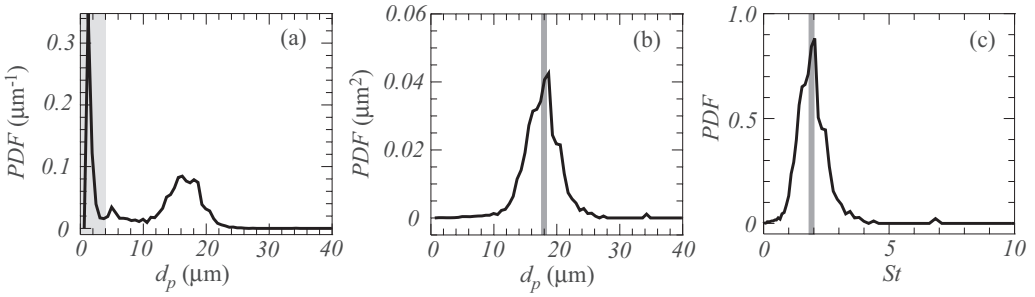

FIG. 5. (a) Probability distribution function (PDF) of droplet diameters, as produced by the spinning disk aerosol generator, and measured using IPI. The large peak at small diameters represents droplets with sizes $d_p \lesssim 5$ μm, that cannot be distinguished with IPI. These diameters have been grayed. (b) PDF of diameters, but now corrected for droplet visibility. (c) PDF of Stokes numbers, also corrected for droplet visibility. The dark gray lines indicate the mean droplet size $d_p = 18$ μm and mean Stokes number St $= 1.9$.

C. Droplets

To create the phosphorescent droplets spinning disk aerosol generator (SDAG) fabricated in house was used. The SDAG idea was first proposed by Walton and Prewett [32], and modifications to it have followed. This type of droplet generators create a relatively monodisperse aerosol and are robust and relatively simple to use.

Interferometric particle imaging (IPI) [33] was used to measure the particle droplet size distribution. The technique is an appealing way of measuring droplet sizes since its setup is relatively simple while yielding two-dimensional data. In a nutshell, the method consists of measuring the interference pattern created by the path length difference between the reflection (zeroth order refraction) and first order refraction of polarized light by a droplet. When imaging out of focus, the interaction between the two different refractions creates interference fringes whose separation can be related to the particle diameter [34]. In out-focus images, each droplet is a disk whose diameter is determined by the focal distance and the size of the camera aperture. The number of interference fringes in this disk is proportional to the droplet size. The diameter of small droplets ($d_p \lesssim 5$ μm) cannot be measured because these droplets produce less than one interference fringe in our setup. A robust algorithm to measure the droplet size probability density function in case of dense droplet collections is explained elsewhere [35]. A typical probability density function P_{d_p} of measured particle diameters is shown in Fig. 5(a). It is well known that a spinning disk aerosol generator not only produces the main droplets with diameter d_p, but also satellite droplets with diameter $\approx d_p/4$. These satellite droplets, whose diameter cannot be measured using IPI, produce the large peak at $d_p \lesssim 5$ μm.

A key advantage of our tagging technique is that the phosphorescent light intensity of a droplet is proportional to its volume, so that the brightness of satellite droplets is approximately two orders of magnitude smaller than that of the main droplets. Therefore, the satellite droplets do not contribute to the measured droplet density field. This is illustrated in Fig. 5(b), where we plot the distribution function corrected for the droplet visibility, $(4/3)\pi(d_p/2)^3 P_{d_p}$. Because the Stokes number is proportional to the square of the droplet radius, even a fairly narrow distribution of droplet sizes results in a large (70%) spread of Stokes numbers, as Fig. 5(c) illustrates.

D. Tagging experiments

To measure the dynamical behavior of preferential concentration we tag the droplets present inside a thin slab within a cloud. This is accomplished by illuminating the droplets with a weakly focused laser sheet (width $\delta_S = 1$ mm), and recording them until their phosphorescence has extinguished using a high-speed camera. The tagging is done using a frequency-tripled pulsed

Nd:YAG laser (Powerlite Precision II 8010, Continuum, Santa Clara, CA) at a rate of 10 Hz and a power output of approximately 120 mJ/pulse. Our field of view is approximately $32 \times 32\,\mathrm{mm}^2$, which translates to a magnification of 64 μm/pixel.

Each realization of the experiment consists of a tagging event and the subsequent recording of 16 images; 3275 realizations are performed to reach convergent statistics. We take cycle averages, such that the averaged quantity depends on the time τ since tagging. The droplet volume fraction is estimated through a balance between the droplet generation rate and the droplet collision rate with the apparatus walls. Our calculations indicate that the volume fraction is on the order of 10^{-7}, so that the droplets do not influence the turbulent flow (one-way coupling).

The images were recorded using an intensified CMOS camera (HiCAM 5000, Lambert Instruments, Roden, The Netherlands). The intensifier is necessary due to the low signal intensity emitted by the glowing droplets coupled with the small exposure inherent to the high frame rate. The camera has a maximum frequency of 5000 FPS with a 512×512 pixel spatial resolution. To counteract the decaying intensity of the glowing droplets we used a field programmable gate array (FPGA) board which externally controlled the intensifier gate time, increasing the exposure time exponentially until a maximum exposure time of 200 μs is reached.

The first (dark) image is recorded before the laser shot, the image after that comes at 0.5 μs after the laser shot. This image sets the origin of time, $\tau = 0$. In each cycle the dark background image (with laser off) is subtracted from the images, and a flat field correction is done by division with the (spatially filtered) cycle-average field at $\tau = 0$.

IV. RESULTS

Our results concern the coarse-grained moments of the droplet density,

$$n_\delta(\boldsymbol{x}, \tau) = \frac{1}{B_\delta} \int_{B_\delta(\boldsymbol{x},\tau)} n(\boldsymbol{x}', \tau)\, d\boldsymbol{x}',$$

with the local density integrated over boxes $B_\delta(\boldsymbol{x}, \tau)$ with side length δ and center $\boldsymbol{x}$. In the Lagrangian frame these boxes move (and deform) with the droplet flow field $\boldsymbol{v}(\boldsymbol{x}, \tau)$; while they are stationary in the Eulerian frame. Positive moments $[n_\delta(\boldsymbol{x}, \tau)]^\alpha$, with $\alpha > 0$, gauge clustering. The fractal dimension is related to the dependence of the average moments on the box size δ. It is a property of the instantaneous droplet density. Time dependence, dynamics, is expressed by the evolution of the moments with time τ. In both cases we use that in our tagging experiments the initial distribution of droplets is in a sheet, so that B_δ are squares with side length δ. In fact, due to the finite sheet width δ_S they are prisms with height δ_S.

A. Fractal dimension

To compute the fractal dimension of the droplet density, we compute the partition sum at time τ, following Halsey *et al.* [36],

$$L(\delta; \alpha) = \sum_i [n_\delta(\boldsymbol{x}_i, \tau)]^\alpha, \tag{4}$$

where the sum $\sum_i$ runs over all squares. This partition sum defines the fractal dimension $D(\alpha)$,

$$L(\delta; \alpha) \sim \delta^{(\alpha-1)D(\alpha)}. \tag{5}$$

For $\alpha = 2$ the dimension is known as the correlation dimension. For a completely homogeneous distribution in a plane, $D^{(2)}(\alpha) = 2$ for all values of α, and where the superscript $^{(2)}$ indicates the dimension of the embedding space (a plane in this case).

The correlation dimension of droplet distributions in a 3D simulated velocity field was reported as $D^{(3)}(2) \simeq 2.4$, [14,16]. However, we are measuring the distribution of droplets in a tagged *sheet*.

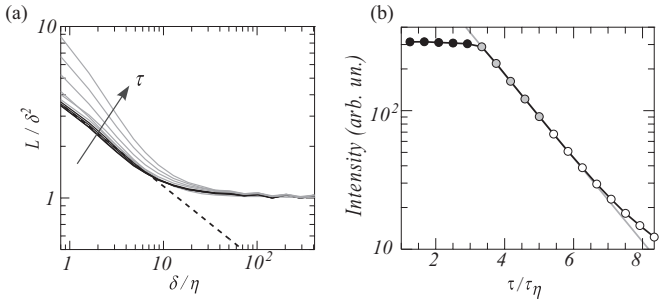

FIG. 6. (a) Scaling of box-integrated intensity, $L(\delta;2)/\delta^2$. In case of a homogeneously filled plane, this quantity would be independent of δ, and would equal 1 because of the chosen normalization. The time delay τ since tagging increases from $\tau/\tau_\eta = 0.05$ to $\tau/\tau_\eta = 2.9$ in steps of $\tau/\tau_\eta = 0.42$. The dashed line fitting the data at $\tau/\tau_\eta = 0.42$ shows $L(\delta;2)/\delta^2 \propto \delta^{-0.45}$, which implies a fractal dimension of the three-dimensional droplet distribution $D(2) \approx 2.5$. However, the fractal scaling does not cover all scales, so that the droplet distribution is not strictly self-similar. For the black lines, the registered phosphorescent intensity is constant due to the exponential stretching of the exposure time, it decays for the gray lines. (b) Mean image intensity as a function of delay time since tagging. During the first five samples the exposure time is stretched such as to compensate for the exponential decay of the phosphorescence. The gray dots correspond to the gray lines in (a). The decay time is $\tau_{\rm ph} = 760\ \mu$s [straight line fit in (b)].

The relation with the fractal scaling of the full three-dimensional droplet distribution is expressed by the intersection rule for fractal dimensions [37]. Let us briefly rephrase this rule for the cover dimension $D = D(0)$. Imagine we cover the three-dimensional droplet distribution with boxes with side length δ. The number of non-empty boxes scales as $\delta^{-D^{(3)}}$, where $D^{(3)}$ is the fractal dimension measured in three dimensional space. Consequently, the chance to find a non-empty box is $P(\delta) = \delta^{3-D^{(3)}}$. This is the same as the chance to find a non-empty square in a two-dimensional intersecting sheet, $\delta^{2-D^{(2)}}$. Therefore, the fractal dimension in the intersection $D^{(2)} = D^{(3)} - 1$. The intersection would be empty when $D^{(3)} < 1$. Using this intersection rule, the corresponding dimension in a sheet intersecting the numerically simulated droplet distribution would be $D^{(2)}(2) - 1 = 1.4$.

Instead of the partition sum $L(\delta;\alpha = 2)$, we compute the deviation from plane filling $L(\delta;\alpha = 2)/\delta^2$. If the tagged droplets would fill the sheet homogeneously, this quantity would be independent of δ.

In Fig. 6 we show $L(\delta;2)/\delta^2$ for increasing time delay τ since tagging. At small distances $\delta/\eta \lesssim 10$, we find scaling with a fractal dimension $D^{(2)}(2) \approx 1.5$. In three dimensions this would amount to $D^{(3)}(2) = 2.5$, which agrees reasonably well with the dimensions found by Bec *et al.* [16] and Calzavarini *et al.* [14]. As also found by the latter authors, the fractal scaling does not cover all scales. The length scale of clusters and voids depends of the Stokes number. For $\mathrm{St} = \mathcal{O}(1)$, the length scale lies in the dissipative range; larger length scales are reached at larger Stokes numbers.

A caveat is that the intersecting sheet in our experiment is not infinitely thin; its width is $\delta_S \approx 10\ \eta$. With the dimension $D^{(3)} \approx 2.4$ found in numerics, we would have found the trivial scaling $L \propto \delta^2$ for $\delta \ll \delta_S$. Clearly, scaling arguments may not capture well clustering of droplets at small scales.

The result in Fig. 6 is shown for several time delays since tagging. As time progresses, the intensity of the glowing drops may sink below the camera intensity threshold, resulting in increasing sparseness of the apparent droplet distribution. As this may affect the appearance of voids and clusters, the decay of the phosphorescence was compensated by stretching the exposure time. This could be done for the first five frames since tagging, after which the exposure time becomes the interframe time. The resulting mean image intensity is shown in Fig. 6(b). The scaling function only starts to change significantly once the intensity starts to decrease.

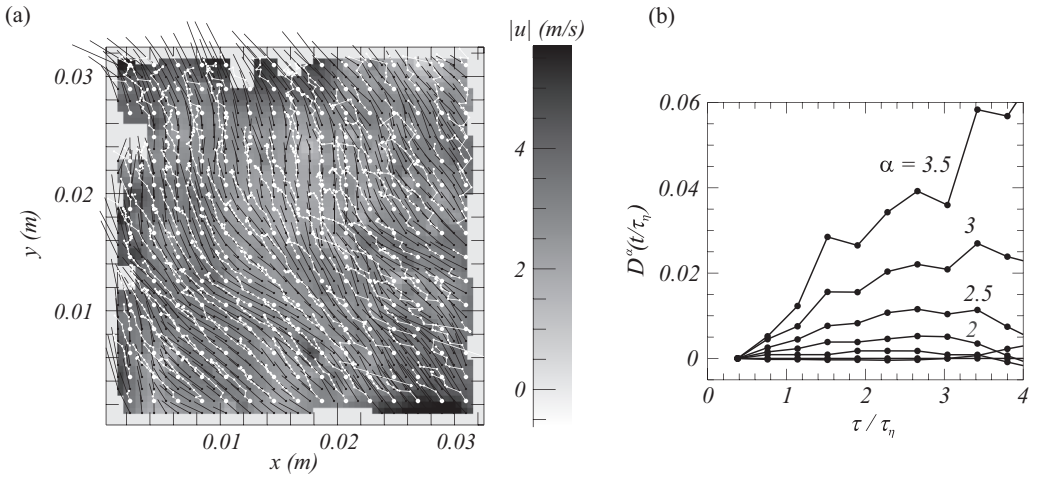

FIG. 7. (a) Tracks used for the Lagrangian measurement of cluster moments (only one out of two tracks is shown). The white dot indicates the starting point. Also shown is the vector displacement field corresponding to $\boldsymbol{v}$ at $\tau = 0$, together with its absolute value. The droplet distribution is not optimal for PIV. (b) Difference between Lagrangian and Eulerian statistics of droplet density moments $\langle (n_\delta(\tau))^\alpha \rangle_L / \langle (n_\delta(\tau))^\alpha \rangle_E - 1$, with $\delta = 12\eta$ and $\alpha = 0.5 \ldots 3.5$.

B. Clustering dynamics

While the fractal dimension is a property of the instantaneous droplet density, we will now study the temporal evolution of the moments $\langle (n_\delta(\tau))^\alpha \rangle$, both in the Eulerian and the Lagrangian frame. The Lagrangian frame was found from planar particle image velocimetry (PIV) using two subsequent images of evolving sheets. We used interrogation windows of 32×32 pixels ($23\eta \times 23\eta$) with a 50 % overlap region. Outliers were detected and replaced through bilinear interpolation [38]. The tagged droplet density is not optimal for accurate particle image velocimetry of $\boldsymbol{v}(\boldsymbol{x}, \tau)$. However, as Fig. 7(a) illustrates, it allows for a fair estimate of the droplet tracks. Displacement errors increase with τ as the phosphorescence dies out. We believe nevertheless that this procedure allows for an adequate distinction between Eulerian and Lagrangian statistics.

Figure 7(b) shows the difference between Lagrangian and Eulerian statistics,

$$D^\alpha(\tau) = \frac{\langle (n_\delta(\tau))^\alpha \rangle_L}{\langle (n_\delta(\tau))^\alpha \rangle_E} - 1,$$

for $\delta = 12\eta$, and moments ranging from $\alpha = 0.5$ to $\alpha = 3.5$. The results show that there is a small but significant preference for cluster growth in the Lagrangian frame. The time interval is short, $\tau \lesssim 4\tau_\eta$. At times much longer than the correlation time of the turbulent velocity, density moments are predicted to increase exponentially [18]. These times are out of reach in this experiment, but may well be reachable in experiments where droplets can be tracked over long times.

The effect that we have measured is small, however, while the prediction of Balkovsky *et al.* [18] assumes a homogeneous initial droplet distribution, the droplets in our sheet which were already clustered at the instant of tagging, do not contribute to the (exponential) increase of the density moments $\langle (n_\delta(\tau))^\alpha \rangle_L$. In fact, it is not possible to experimentally realize the condition of Balkovsky *et al.* [18].

V. CONCLUSIONS

Glowing drops make a unique tracer of preferential concentration. In tagged sheetlike volumes containing many droplets—much more than could be traced individually—we have quantified

the two-dimensional concentration field. The droplets generated are fairly monodisperse, with the size distribution of the visualized drops narrowed by the volume weighting by their emitted light intensity. In addition, phosphorescence, much as fluorescence is an effective way to suppress reflected light.

After the initial tagging, the shape of the tagged sheet evolves as it is deformed by turbulent velocity fluctuations. When the sheet is wrinkled strongly, it may lead to (apparent) clustering. The largest deformation is done by by the largest vortices, which have a velocity difference $u = 2$ m/s. During an experiment cycle, lasting $\approx 3\tau_\eta \approx 1.4$ ms, this amounts to a displacement ≈ 3 mm $= 3\,\delta_S$, with δ_S the thickness of the laser sheet. Therefore, wrinkling of the tagged sheet does not explain small-scale clustering. Another dynamic quantity, namely the deformation of narrow ($\approx 10\eta$) pencil-shaped tagged volumes has been studied by us in [4].

Our measurement of clustering dynamics is a proof of principle. It illustrates how a relevant dynamical quantity can be extracted from time-dependent data of droplet fields. We are looking forward to measurements of the same quantity in cases where the full three-dimensional droplet field can be tracked over long times.

ACKNOWLEDGMENTS

This work is part of the research program of the "Stichting voor Fundamenteel Onderzoek der Materie (FOM)," which is financially supported by the "Nederlandse Organisatie voor Wetenschappelijk Onderzoek (NWO)." This work is also supported by the COST Action No. MP0806.

[1] R. A. Shaw, Particle-turbulence interactions in atmospheric clouds, Annu. Rev. Fluid Mech. **35**, 183 (2003).
[2] F. Toschi and E. Bodenschatz, Lagrangian properties of particles in turbulence, Annu. Rev. Fluid Mech. **41**, 375 (2009).
[3] S. Balachandar and J. K. Eaton, Turbulent dispersed multiphase flow, Annu. Rev. Fluid Mech. **42**, 111 (2010).
[4] H. Bocanegra Evans, N. Dam, G. Bertens, D. van der Voort, and W. van de Water, Dispersion of Droplet Clouds in Turbulence, Phys. Rev. Lett. **117**, 164501 (2016).
[5] M. R. Maxey, The gravitational settling of aerosol particles in homogeneous turbulence and random flow fields, J. Fluid Mech. **174**, 441 (1987).
[6] K. D. Squires and J. K. Eaton, Prefential concentration of particles by turbulence, Phys. Fluids A **3**, 1169 (1991).
[7] S. Ayyalasomayajula, Z. Warhaft, and L. R. Collins, Modeling inertial particle acceleration statistics in isotropic turbulence, Phys. Fluids **20**, 095104 (2008).
[8] G. Falkovich, A. Fouxon, and M. G. Stepanov, Acceleration of rain initiation by cloud turbulence, Nature **419**, 151 (2002).
[9] M. Wilkinson and B. Mehlig, Caustics in turbulent aerosols, Europhys. Lett. **71**, 186 (2005).
[10] G. P. Bewley, E.-W. Saw, and E. Bodenschatz, Observation of the sling effect, New J. Phys. **15**, 083051 (2013).
[11] E. Saw, R. Shaw, S. Ayyalasomayajula, P. Chuang, and Á. Gylfason, Inertial Clustering of Particles in High-Reynolds-Number Turbulence, Phys. Rev. Lett. **100**, 214501 (2008).
[12] E.-W. Saw, R. Shaw, J. P. L. C. Salazar, and L. R. Collins, Spatial clustering of polydisperse inertial particles in turbulence: II. Comparing simulation with experiment, New J. Phys. **14**, 105031 (2012).
[13] J. P. L. C. Salazar, J. De Jong, L. Cao, S. H. Woodward, H. Meng, and L. R. Collins, Experimental and numerical investigation of inertial particle clustering in isotropic turbulence, J. Fluid Mech. **600**, 245 (2008).
[14] E. Calzavarini, M. Kerscher, D. Lohse, and F. Toschi, Dimensionality and morphology of particle and bubble clusters in turbulent flow, J. Fluid Mech. **607**, 13 (2008).

[15] J. L. Kaplan and J. A. Yorke, Chaotic behavior of multidimensional difference equations, in *Functional Differential Equations and Approximations of Fixed Points*, edited by H. O. Peitgen and H. O. Walther (Springer, Berlin, 1979), Vol. 703, pp. 204–227.
[16] J. Bec, L. Biferale, M. Cencini, A. Lanotte, S. Musacchio, and F. Toschi, Heavy Particle Concentration in Turbulence at Dissipative and Inertial Scales, Phys. Rev. Lett. **98**, 084502 (2007).
[17] R. Monchaux, M. Bourgoin, and A. Cartellier, Preferential concentration of heavy particles: A Voronoï analysis, Phys. Fluids **22**, 103304 (2010).
[18] E. Balkovsky, G. Falkovich, and A. Fouxon, Intermittent Distribution of Inertial Particles in Turbulent Flows, Phys. Rev. Lett. **86**, 2790 (2001).
[19] W. R. Lempert, P. Ronney, and K. Magee, Flow tagging velocimetry in incompressible flow using photo-activated nonintrusive tracking of molecular motion (PHANTOMM), Exp. Fluids **18**, 249 (1995).
[20] R. B. Miles, C. Cohen, J. J. Connors, P. J. Howard, S. Huang, E. C. Markovitz, and G. Russell, Velocity measurements by vibrational tagging and fluorescent probing of oxygen, Opt. Lett. **12**, 861 (1987).
[21] A. Noullez, G. Wallace, W. Lempert, R. B. Miles, and U. Frisch, Transverse velocity increments in turbulent flow using the relief technique, J. Fluid Mech. **339**, 287 (1997).
[22] N. Dam, R. J. H. Klein-Dowel, N. M. Sijtsema, and J. J. ter Meulen, Nitric oxide flow tagging in unseeded air, Opt. Lett. **26**, 36 (2001).
[23] J. Bominaar, M. Pashtrapanska, T. Elenbaas, N. Dam, H. ter Meulen, and W. van de Water, Writing in turbulent air, Phys. Rev. E **77**, 046312 (2008).
[24] M. M. Koochesfahani and D. G. Nocera, Molecular Tagging Velocimetry, in *Springer Handbook of Experimental Fluid Mechanics*, edited by C. Tropea, A. Yarin, and F. J. Foss (Springer Verlag, Berlin, 2007), Chap. 5.4.
[25] S. Krüger and G. Grünefeld, Droplet velocity and acceleration measurements in dense sprays by laser flow tagging, Appl. Phys. B **71**, 611 (2000).
[26] E. F. G. Dickson, A. Pollak, and E. P. Diamandis, Time-resolved detection of lanthanide luminescence for ultrasensitive bioanalytical assays, J. Photochem. Photobiol. B **27**, 3 (1995).
[27] N. Arnaud and J. Georges, Comprehensive study of the luminescent properties and lifetimes of Eu^{3+} and Tb^{3+} chelated with various ligands in aqueous solutions: Influence of the synergic agent, the surfactant and the energy level of the ligand triplet, Spectrochim. Acta A **59**, 1829 (2003).
[28] W. Hwang and J. K. Eaton, Creating homogeneous and isotropic turbulence without a mean flow, Exp. Fluids **36**, 444 (2004).
[29] J. Sheng, H. Meng, and R. O. Fox, A large eddy PIV method for turbulence dissipation rate estimation, Chem. Eng. Sci. **55**, 4423 (2000).
[30] G. Bertens, D. van der Voort, and W. van de Water, Large-eddy estimate of the turbulent dissipation rate using piv, Exp. Fluids **56**, 89 (2015).
[31] J. Smagorinsky, General circulation experiments with the primitive equations, I. The basic experiment.Mon. Weather Rev. **91**, 99 (1963).
[32] W. H. Walton and W. C. Prewett, The production of sprays and mists of uniform drop size by means of spinning disc type sprayers, Proc. Phys. Soc. London, Sect. B **62**, 341 (1949).
[33] G. König, K. Anders, and A. Frohn, A new light-scattering technique to measure the diameter of periodically generated moving droplets, J. Aerosol Sci. **17**, 157 (1986).
[34] H.-E. Albrecht, M. Borys, N. Damaschke, and C. Tropea, *Laser Doppler and Phase Doppler Measurement Techniques* (Springer Verlag, Berlin, 2003).
[35] H. Bocanegra Evans, N. Dam, D. van der Voort, G. Bertens, and W. van de Water, Measuring droplet size distributions from overlapping interferometric particle images, Rev. Sci. Instrum. **86**, 023709 (2015).
[36] T. C. Halsey, M. H. Jensen, L. P. Kadanoff, I. Procaccia, and B. I. Shraiman, Fractal measures and their singularities: The characterization of strange sets, Phys. Rev. A **33**, 1141 (1986).
[37] B. B. Mandelbrot, *The Fractal Geometry of Nature* (W.H. Freeman, San Francisco, 1983), p. 468.
[38] J. Westerweel and F. Scarano, Universal outlier detection for PIV data, Exp. Fluids **39**, 1096 (2005).